PLOS ONE

Slow Receptor Dissociation Kinetics Differentiate Macitentan from Other Endothelin Receptor Antagonists in Pulmonary Arterial Smooth Muscle Cells

John Gatfield*, Celia Mueller Grandjean, Thomas Sasse, Martine Clozel, Oliver Nayler

Actelion Pharmaceuticals Ltd., Allschwil, Switzerland

Abstract

Two endothelin receptor antagonists (ERAs), bosentan and ambrisentan, are currently approved for the treatment of pulmonary arterial hypertension (PAH), a devastating disease involving an activated endothelin system and aberrant contraction and proliferation of pulmonary arterial smooth muscle cells (PASMC). The novel ERA macitentan has recently concluded testing in a Phase III morbidity/mortality clinical trial in PAH patients. Since the association and dissociation rates of G protein-coupled receptor antagonists can influence their pharmacological activity in vivo, we used human PASMC to characterize inhibitory potency and receptor inhibition kinetics of macitentan, ambrisentan and bosentan using calcium release and inositol-1-phosphate (IP_1) assays. In calcium release assays macitentan, ambrisentan and bosentan were highly potent ERAs with K_b values of 0.14 nM, 0.12 nM and 1.1 nM, respectively. Macitentan, but not ambrisentan and bosentan, displayed slow apparent receptor association kinetics as evidenced by increased antagonistic potency upon prolongation of antagonist pre-incubation times. In compound washout experiments, macitentan displayed a significantly lower receptor dissociation rate and longer receptor occupancy half-life ($ROt_{1/2}$) compared to bosentan and ambrisentan ($ROt_{1/2}$:17 minutes versus 70 seconds and 40 seconds, respectively). Because of its lower dissociation rate macitentan behaved as an insurmountable antagonist in calcium release and IP_1 assays, and unlike bosentan and ambrisentan it blocked endothelin receptor activation across a wide range of endothelin-1 (ET-1) concentrations. However, prolongation of the ET-1 stimulation time beyond $ROt_{1/2}$ rendered macitentan a surmountable antagonist, revealing its competitive binding mode. Bosentan and ambrisentan behaved as surmountable antagonists irrespective of the assay duration and they lacked inhibitory activity at high ET-1 concentrations. Thus, macitentan is a competitive ERA with significantly slower receptor dissociation kinetics than the currently approved ERAs. Slow dissociation caused insurmountable antagonism in functional PASMC-based assays and this could contribute to an enhanced pharmacological activity of macitentan in ET-1-dependent pathologies.

Introduction

Pulmonary arterial hypertension (PAH) is a rare and severe disease that is characterized by increased pressure in the pulmonary circulation caused by progressive pulmonary artery remodeling and constriction of the pulmonary vasculature [1]. The initiating cause of this devastating disease is largely unknown; however, pulmonary endothelial dysfunction and smooth muscle cell abnormality are significant contributors [2].

Treatments that aim at restoring the balance of endothelium-derived vasoactive substances are effective in reducing pulmonary vascular resistance and increasing exercise capacity [3,4,5]. Such treatments comprise prostacyclin analogues, phosphodiesterase type 5 inhibitors and endothelin receptor antagonists (ERAs). Endothelin (ET) concentrations are elevated in lung tissue of PAH patients [6] and the central pathogenic role of ET in PAH has

been demonstrated in several clinical trials evaluating different ERAs [7].

Endothelins are vasoactive peptides of which endothelin-1 (ET-1) is the most abundant in lung tissue [8]. ET-1 is the most potent and long lasting vasoconstrictor known in man, and it acts as mitogen, angiogenic factor, mediator of fibrosis and inflammation. All of these processes are aberrantly activated in pulmonary vessels in PAH [9,10,11,12,13]. ET-1 responses are mediated via activation of two homologous G protein-coupled receptor subtypes, endothelin A receptor (ET_A) and endothelin B receptor (ET_B) [14,15]. Both receptor subtypes activate $G\alpha q$ protein-mediated pathways leading to phospholipase $C\beta$ activation and increased intracellular calcium concentrations [16].

Endothelial cells are the main source of ET-1 and they secrete this peptide via two routes. The constitutive pathway is thought to contribute to basal vascular tone whereas the non-constitutive pathway releases ET-1 in response to a variety of external stimuli

from specialized storage vesicles [17,18]. Consistent with its site of action, ET-1 secretion by endothelial cells is polarized towards the basolateral space, i.e. into the deeper tissues of the vessel wall [19]. The secretion of endothelial ET-1 is triggered by stimuli such as hypoxia, growth factors, cytokines, steroids, flow/shear stress and vessel injury [20,21,22,23,24,25]. In the lung, changes in local ET -1 concentration are then sensed by neighboring pulmonary arterial smooth muscle cells (PASMC) and fibroblasts expressing ET receptors. In PASMC, ET receptors are coupled to the $G\alpha q$ pathway and activate phospholipase $C\beta$ and inositol-trisphosphate (IP_3) and diacylglycerol production. These early second messengers initiate a biphasic calcium response resulting in sustained elevation of intracellular calcium levels. Elevated calcium levels promote of cytoskeletal contraction and cell proliferation [7,16] and thereby mediate persistent vasoconstriction and vascular remodeling, both central pathological processes in PAH [26,27,28,29].

In the present study we used second messenger assays in primary human PASMC to characterize ET receptor association and dissociation kinetics of macitentan, a novel ERA [30], in comparison with bosentan and ambrisentan, the two ERAs approved for the treatment of PAH. Macitentan had a slow apparent receptor association rate and a 15-fold extended receptor occupancy half-life ($ROt_{1/2}$) compared to bosentan and ambrisentan. Consequently, macitentan, but neither bosentan nor ambrisentan, displayed insurmountable antagonism in cellular assays with short incubation times and blocked ET receptor activation irrespective of the added ET-1 concentration. Since blockade of ET receptor signaling in PASMC is a key aspect of successful therapeutic intervention in PAH, the unique kinetic properties of macitentan may allow a more effective treatment of the ET-1-mediated pathological hemodynamic and structural effects in PAH and other diseases.

Results

Contribution of Endothelin Receptor Subtypes to Signaling in PASMC

Cultured human primary PASMC, a central therapeutic target cell in PAH, expressed high levels of ET_A mRNA and considerably less ET_B mRNA (unpublished data and [28]). A set of five reference ERAs with different receptor subtype selectivity profiles was used to determine if the different receptor subtype mRNA expression levels were also reflected in the relative ET_A and ET_B receptor contribution to ET-1-induced calcium signaling. The antagonist K_b values obtained in PASMC were compared with K_b values generated in CHO cells expressing either the recombinant ET_A receptor or the recombinant ET_B receptor. To this end, antagonist dilution series were pre-incubated for 120 min with the respective cell types, which were then stimulated with ET-1 (EC_{50}–EC_{70}). Fluorescence traces were recorded for 3 min in the fluorescence imaging plate reader (FLIPR), and peak fluorescence values were used to calculate half maximum inhibitory concentrations of the antagonists (IC_{50}). These were then transformed into functional inhibition constants (K_b) using the Cheng-Prusoff equation [31] (see Methods). As shown in table 1, in recombinant cells, the dual ET_A/ET_B receptor antagonist tezosentan displayed mixed ET_A and ET_B antagonism while the ET_A receptor antagonists BQ-123, sitaxentan and zibotentan selectively blocked ET_A receptors and the ET_B receptor antagonist BQ-788 selectively blocked ET_B receptors. In PASMC, the compounds covered a range of antagonistic potencies ranging from $K_b = 10$ pM for tezosentan to $K_b = 117$ nM for BQ-788. To assess the receptor subtype contribution to ET-1-induced signaling

in human PASMC, the K_b values obtained in PASMC were compared with K_b values obtained in the CHO-ET_A system (Fig. 1A) or in the CHO-ET_B system (Fig. 1B). A significant correlation ($R^2 = 0.990$) was obtained with CHO-ET_A data, while no correlation ($R^2 = 0.004$) was seen with the CHO-ET_B data, suggesting that the ET_A receptor was the main mediator of ET-1-induced calcium release in these PASMC. A general shift to lower antagonistic potency was observed in the CHO-ET_A system, possibly due to receptor over-expression and a higher receptor reserve in the recombinant system. Tab. 1 summarizes these K_b data.

Antagonistic Potency and Apparent Association Kinetics of Different ERAs

Macitentan was compared with different known ERAs, including ambrisentan and bosentan, with respect to potency and apparent association kinetics in PASMC. The cells were pre-incubated with ERA dilution series for either 10 min or 120 min (steady state condition) and the resulting calcium signals were measured after stimulation with ET-1. The calculated K_b values for each compound and each incubation condition (Table 2 and Fig. 2) illustrate that all tested ERAs, with the exception of macitentan and to a lower extent of tezosentan, reached steady state after 10 min, as evidenced by the lack of potency shift when the pre-incubation time was extended from 10 min to 120 min. Macitentan however, displayed a 6.3-fold increase in potency after 120 min, compared to 10 min pre-incubation, indicating slow apparent association kinetics. In terms of potency ambrisentan and macitentan were similar at steady state after 120 min of pre-incubation ($K_{b\_maci} = 0.12$ nM, $K_{b\_ambri} = 0.14$ nM) while bosentan was approximately 10-fold less potent ($K_{b\_bosent} = 1.1$ nM).

Dissociation Kinetics and Receptor Occupancy Half-life of Macitentan, Ambrisentan and Bosentan

Slow apparent association kinetics can be caused by an increased receptor occupancy half-life ($ROt_{1/2}$) and slow dissociation. Therefore, we determined the $ROt_{1/2}$ of macitentan, bosentan and ambrisentan in PASMC using functional readouts after antagonist washout. PASMC were incubated with increasing concentrations of macitentan, ambrisentan or bosentan for 120 min and the cells were then either directly stimulated with ET-1 or subjected to a washout procedure to eliminate free compound. Following the washout procedure the cells were stimulated with an EC_{50}–EC_{70} of ET-1 after different recovery times and calcium release was measured (Fig. 3). The IC_{50} values at the different time points were calculated and converted via the Cheng-Prusoff equation ($K_b = IC_{50}/(1+ [ET-1_{stim}]/EC_{50\_ET-1})$) to K_b values [31] using the EC_{50} of ET-1 determined on the same assay plate as well as the stimulating ET-1 concentration. At low stimulating ET-1 concentrations this calculation gives a good estimate of the K_b value even for insurmountable antagonists [32]. Five minutes after the compound was washed out, ambrisentan- and bosentan-treated PASMC had already regained their responsiveness to ET-1 stimulation, as evidenced by statistically significant shifts in K_b by factors of $\sim$170 (ambrisentan) and $\sim$20 (bosentan). In contrast, macitentan-treated PASMC remained ET-1 unresponsive and a statistically significant shift in K_b was first seen 60 min after washout. These data demonstrate a marked difference in the $ROt_{1/2}$ of macitentan compared to ambrisentan, and bosentan. Based on the shift in K_b at 5 min, a $ROt_{1/2}$ of $\sim$40 seconds (ambrisentan) and $\sim$70 seconds (bosentan) was calculated, assuming an exponential drop in receptor blockade over time. The 13-fold loss in potency of macitentan over 60 min

A
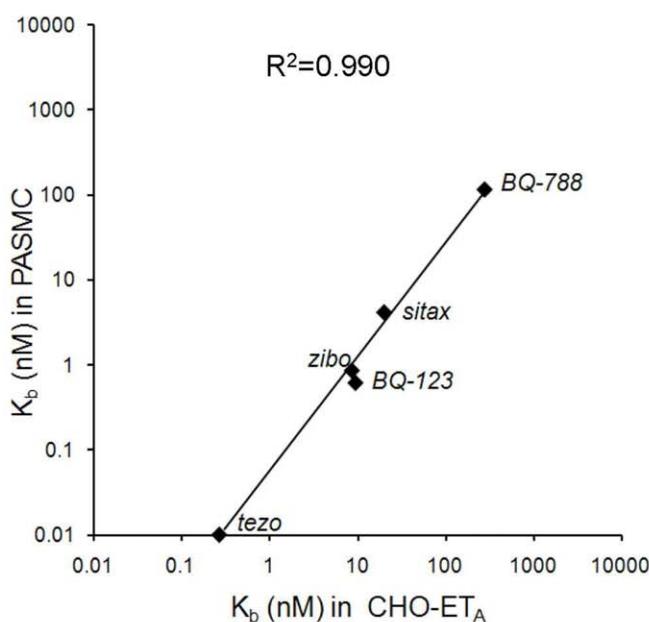
B
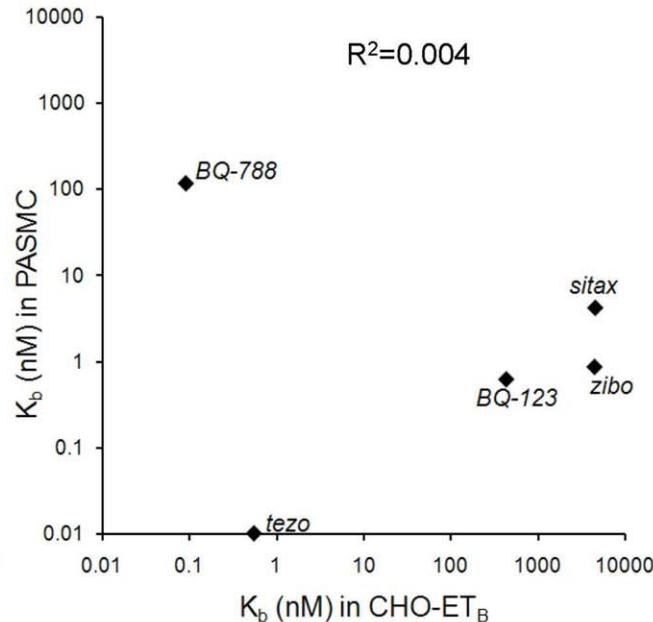
Figure 1. Contribution of endothelin receptor subtypes to calcium signaling in human primary PASMC. PASMC or CHO-ET$_A$ or CHO-ET$_B$ cells were pre-incubated with reference ERA dilution series for 120 min and then stimulated in the FLIPR with ET-1 (EC$_{50}$–EC$_{70}$). IC$_{50}$ values were calculated from fluorescence peak responses and transformed into K$_b$ values as described in Methods. Correlation scatter plot of K$_b$ values obtained in PASMC versus CHO-ET$_A$ cells (A) or versus CHO-ET$_B$ cells (B). The correlation line and R^2 value was generated by linear regression of the double-logarithmic data. Geometric means of n = 3–8 determinations are shown.
doi:10.1371/journal.pone.0047662.g001

translated to a ROt$_{1/2}$ of ~17 min. Taken together, macitentan showed a ~15-fold increased ROt$_{1/2}$ compared to ambrisentan and bosentan.

Consequences for Mode of ET Receptor Antagonism

Compounds with increased ROt$_{1/2}$ such as macitentan can behave as insurmountable antagonists when using agonist stimulation times that are shorter than the ROt$_{1/2}$ of the antagonist-receptor complex [32]. IP$_1$ accumulation assays are well suited to vary agonist stimulation times due to a long-lasting signal development and they are therefore often used to investigate the mode of antagonism of Gαq-coupled G protein coupled receptors. To assess whether macitentan, ambrisentan and bosentan differ in their mode of antagonism, concentration-

Table 1. Mean K$_b$ values for reference ERAs determined by calcium release assays in CHO-ET$_A$, CHO-ET$_B$ and human PASMC.

	K$_b$ (nM)*		
	CHO-ET$_A$	CHO-ET$_B$	PASMC
BQ-123	9.4	425	0.62
BQ-788	277	0.090	117
sitaxentan	20	4468	4.2
tezosentan	0.26	0.50	0.010
zibotentan	8.5	4389	0.87

*geometric means from n = 3–8 determinations calculated from IC$_{50}$ values via Cheng-Prusoff equation (see Methods).
doi:10.1371/journal.pone.0047662.t001
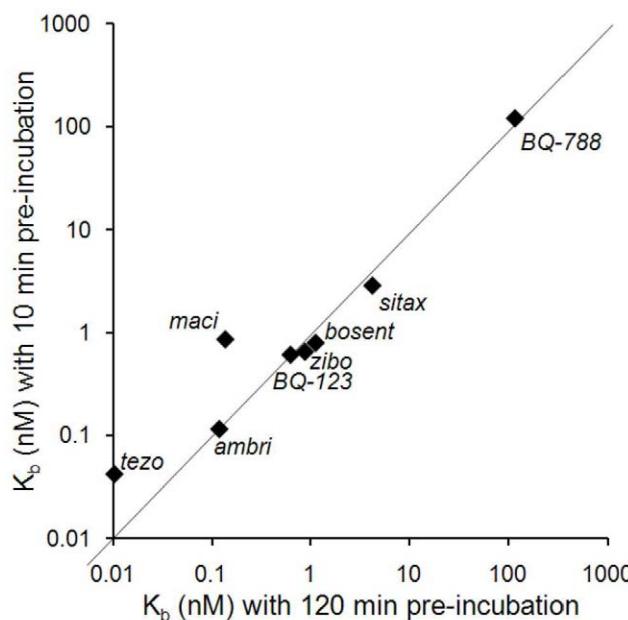
Figure 2. Antagonistic potency and apparent association kinetics of different ERAs using calcium release assays in PASMC. Cells were pre-incubated with antagonist dilution series for 10 min or 120 min and then stimulated in the FLIPR with ET-1 (EC$_{50}$–EC$_{70}$). IC$_{50}$ values were calculated from fluorescence peak responses and transformed into K$_b$ values as described in Methods. Correlation scatter plot of the K$_b$ values generated for 10 min versus 120 min antagonist pre-incubation times (geometric means of n = 6 determinations).
doi:10.1371/journal.pone.0047662.g002

Table 2. Mean K_b values for different ERAs determined by calcium release assays in human PASMC with 10 min or 120 min antagonist pre-incubation time.

	K_b (nM) 10 min*	K_b (nM) 120 min*	K_b ratio
ambrisentan	0.11	0.12	1.0
bosentan	0.79	1.1	0.7
BQ-123	0.61	0.62	1.0
BQ-788	121	117	1.0
macitentan	0.86	0.14	6.3
sitaxentan	2.9	4.2	0.7
tezosentan	0.042	0.010	4.1
zibotentan	0.65	0.87	0.7

*geometric means of n = 6 determinations calculated from IC_{50} values via Cheng-Prusoff equation (see Methods).
doi:10.1371/journal.pone.0047662.t002

response curves (CRCs) of ET-1 were generated in the presence of increasing concentrations of the three ERAs (Schild analysis), and IP_1 accumulation was determined after 20 min of ET-1 stimulation. All three antagonists concentration-dependently blocked ET-1-induced IP_1 accumulation in PASMC (Fig. 4). However, while ambrisentan and bosentan showed a surmountable mode of antagonism causing equidistant rightward shifts in the ET-1 CRCs, macitentan displayed an insurmountable mode of antagonism with a depression of maximum response in addition to rightward shifts in the ET-1 CRCs. Thus, the increased $ROt_{1/2}$ of macitentan was associated with an insurmountable antagonism.

The IP_1 accumulation assay data was also used to deduce K_b values for the different antagonists via the Cheng-Prusoff equation. Again, for K_b calculations we used the IC_{50} values that were generated at the lowest ET-1 concentration that delivered a robust signal strength (1.6 nM ET-1). Ambrisentan (K_b: 1.1 nM,

$\sigma_g = 1.6$, n = 4) and macitentan (K_b: 0.74 nM, $\sigma_g = 1.4$, n = 4) showed similar potency and both were approximately 10-fold more potent than bosentan (K_b: 12 nM, $\sigma_g = 2.2$, n = 4) with σg being the geometric standard deviation. These results were therefore in line with the data obtained by calcium flux assays in human PASMCs.

To differentiate slow-offset orthosteric antagonism from irreversible antagonism or allosteric antagonism, we next performed assays with longer stimulation times. Slow-offset antagonists behave as surmountable competitive antagonists in such assays if the stimulation time is significantly longer than the $ROt_{1/2}$ of the antagonist-receptor complex. In contrast, allosteric antagonists or irreversible blockers would not change their mode of inhibition upon prolonged incubation. The IP_1 accumulation assay was therefore performed with 20 minutes and with 90 minutes of ET-1 stimulation time, the latter being well beyond the estimated $ROt_{1/2}$ of ∼ 17 min for macitentan and allowing for better antagonist-agonist equilibration. Macitentan displayed insurmountable antagonism with 20 minutes incubation time (Fig. 5A) and surmountable antagonism (Fig. 5B) when the stimulation time was prolonged to 90 minutes. In contrast, ambrisentan and bosentan displayed surmountable antagonism irrespective of the incubation time (Fig. 5A,B). Therefore, under equilibrium conditions macitentan revealed its competitive antagonistic mode of action as evidenced by equidistant rightward shifts of the ET-1 CRCs, full surmountability of the antagonism and a lack of saturability of the antagonistic effect that would be seen for negative allosteric modulators.

As surmountable antagonism was seen for all compounds for the 90-minute incubation time Schild K_b values could be calculated. As seen in previous experiments, macitentan (Schild K_b: 1.4, $\sigma_g = 2.1$, n = 3) and ambrisentan (Schild K_b = 1.6 nM, $\sigma_g = 2.3$, n = 3) displayed similar potency and both were approximately 10-fold more potent than bosentan (Schild K_b:16 nM, $\sigma_g = 1.8$, n = 3).

In summary, macitentan was a slow-offset orthosteric antagonist causing an insurmountable antagonism if the assay incubation
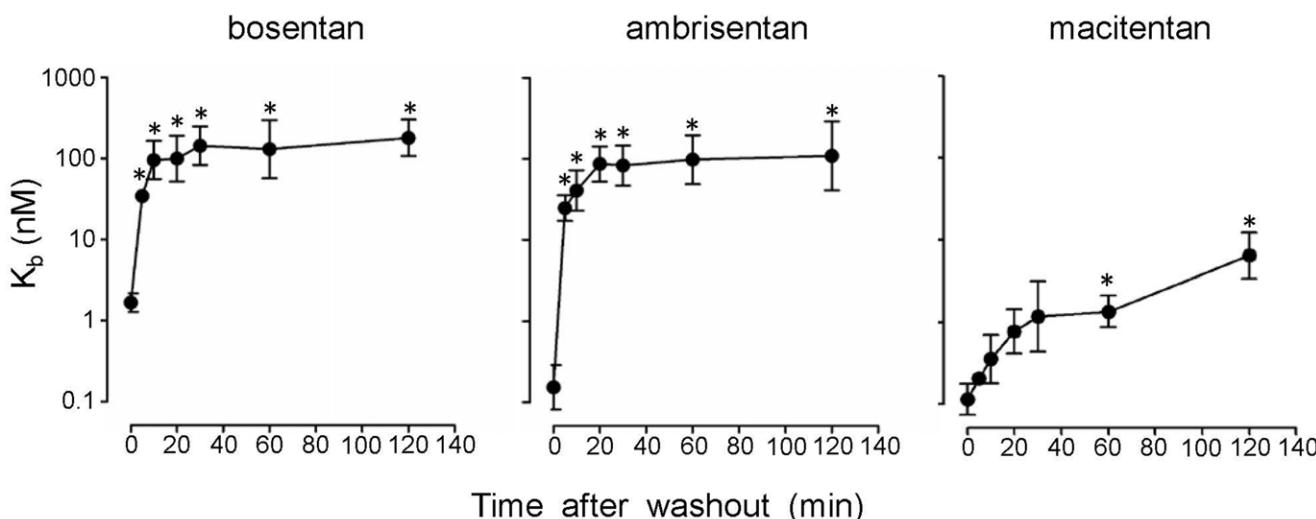
Figure 3. Dissociation kinetics of macitentan, ambrisentan and bosentan determined by calcium release assays in PASMC. Cells were pre-incubated for 120 min with antagonist dilution series and then either directly stimulated with ET-1 (EC_{50}–EC_{70}) or subjected to a compound washout procedure followed by stimulation with ET-1 at the indicated time points after washout. The peak calcium responses were used to calculate IC_{50} values which were transformed into K_b values as described in Methods. Shown are the time-dependent changes in K_b after washout. Geometric means are displayed +/− SEM. K_b values after washout significantly different (p<0.05) from the K_b at 0 min are indicated with an asterisk. Test: one-way ANOVA, Dunnett's post test.
doi:10.1371/journal.pone.0047662.g003
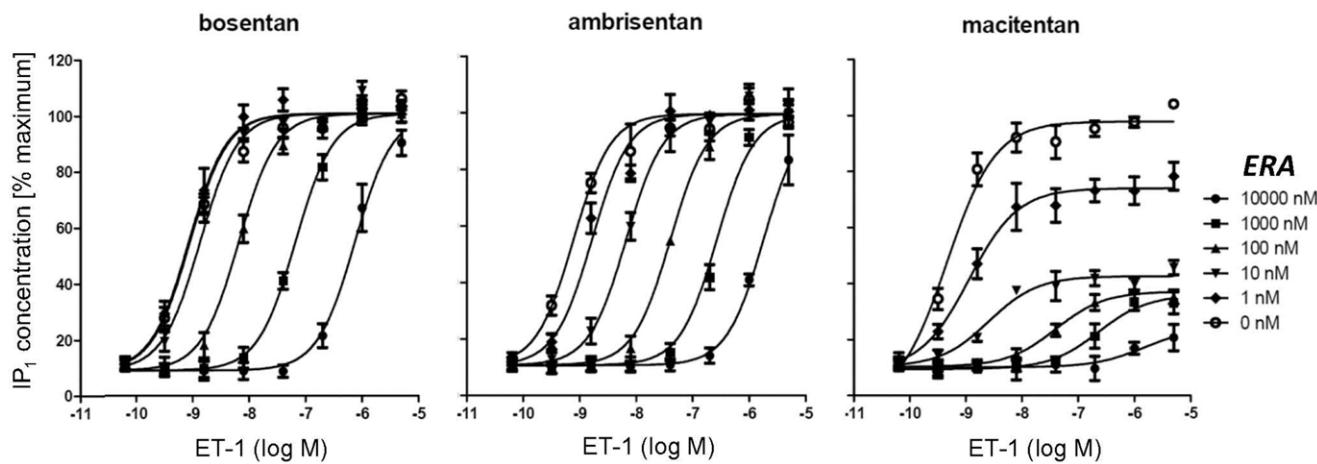
Figure 4. Effect of bosentan, ambrisentan and macitentan on ET-1-induced IP$_1$ accumulation. Human PASMCs were pre-incubated with dilution series of antagonists for 120 min followed by the addition of a dilution series of ET-1. After 20 min of stimulation, cells were lysed and the IP$_1$ content was determined. Raw data from 4 independent experiments were normalized, and average values +/− SEM are shown.
doi:10.1371/journal.pone.0047662.g004
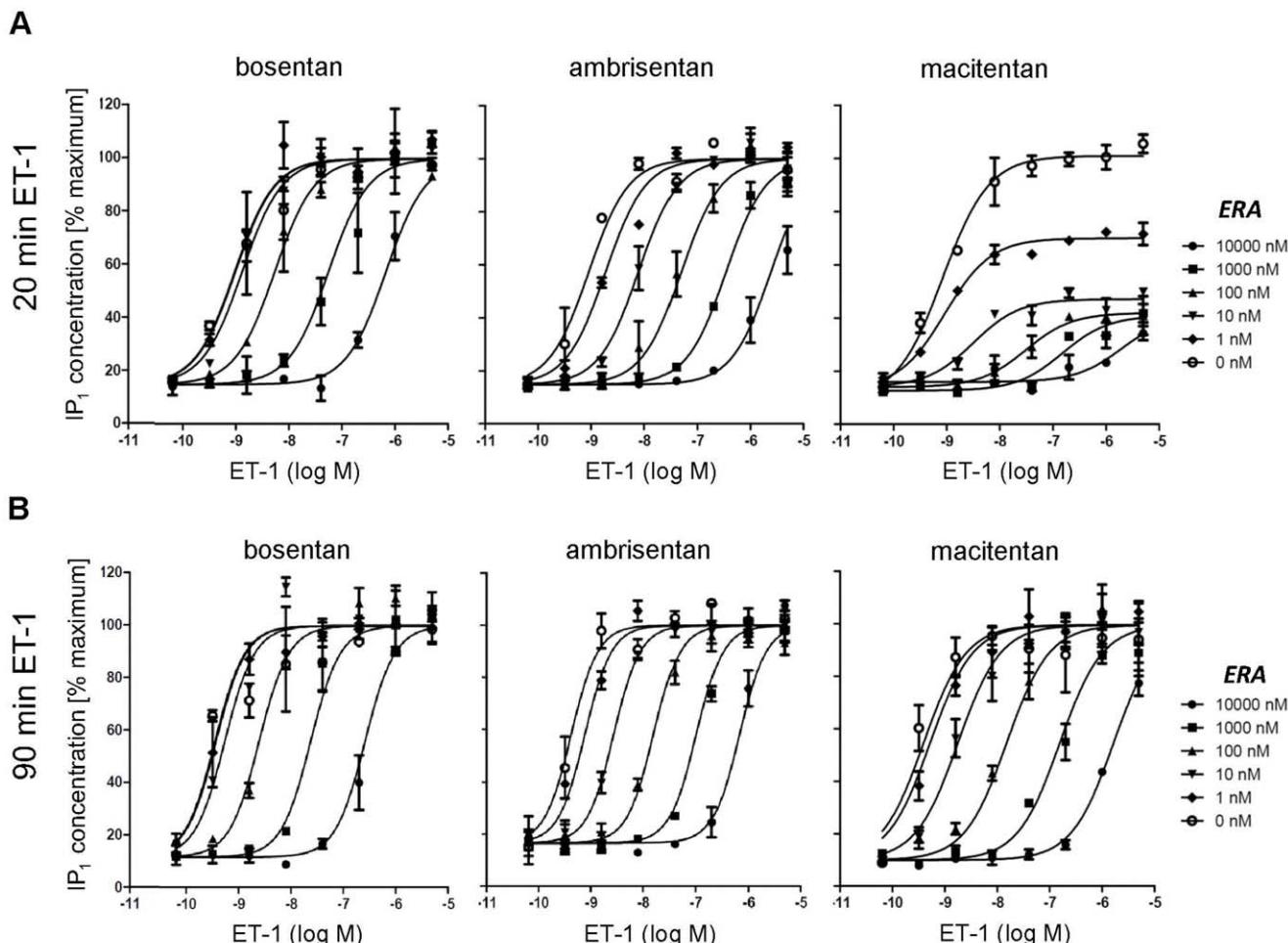
Figure 5. Time dependence of macitentan insurmountability determined in IP$_1$ accumulation assays. Human PASMCs were pre-incubated with dilution series of antagonists for 120 min followed by the addition of a dilution series of ET-1. After 20 min (A) or 90 min (B) of stimulation, cells were lysed and the IP$_1$ content was determined. Shown are the raw data +/− SD of duplicates of one representative experiment of a total of n = 3.
doi:10.1371/journal.pone.0047662.g005

time was shorter than the calculated $ROt_{1/2}$ but a surmountable antagonism was observed if the assay time was longer than the calculated $ROt_{1/2}$. In contrast, both ambrisentan and bosentan showed surmountable antagonism irrespective of the ET-1 stimulation times.

The calcium release induced in PASMC by ET-1 is characterized by a biphasic profile consisting of a rapid transient increase and a second sustained elevation [33,34,35], the latter being associated with sustained contraction and cell proliferation in pathology [29,36]. We used these two response phases to further evaluate the three ERAs ambrisentan, bosentan and macitentan. In PASMC, ET-1 stimulation caused a robust, transient increase in cytosolic calcium, which peaked 30 seconds after ET-1 addition and lasted for about 3 min. It was followed by a second, prolonged but less pronounced increase in cytosolic calcium, which lasted for more than 25 min (Fig. 6A). Both phases showed a concentration-dependent, saturable behavior (Fig. 6B and C).

Macitentan, ambrisentan and bosentan were investigated in Schild experiments with 120-min pre-incubation times and the effects on the two phases of calcium increase were analyzed independently. The first response phase was quantified by using the fluorescence peak height within the first 3 minutes, and the second phase was quantified by calculating the area under the curve between 3 minutes and 23 minutes of observation.

Due to the fast signal development of the first calcium response (30 seconds to peak), all three compounds displayed a certain degree of insurmountable antagonism as expected, although macitentan was the most pronounced (Fig.7A). The extent of insurmountability was further illustrated by displaying the ERA inhibition curves at a fixed ET-1 concentration (1 μM). For ambrisentan and bosentan these curves were biphasic (Fig.7B) and reached an intermediate plateau of antagonistic efficacy with the residual unblocked signal being descriptive of the proportion of receptor that is subject to surmountable antagonism [37]. In fact, bosentan showed a surmountable mode of antagonism for ~50% of the ET-1-induced signal and ambrisentan showed this surmountable mode for ~30% of the ET-1-induced signal. Macitentan showed no surmountable behavior. Therefore, based
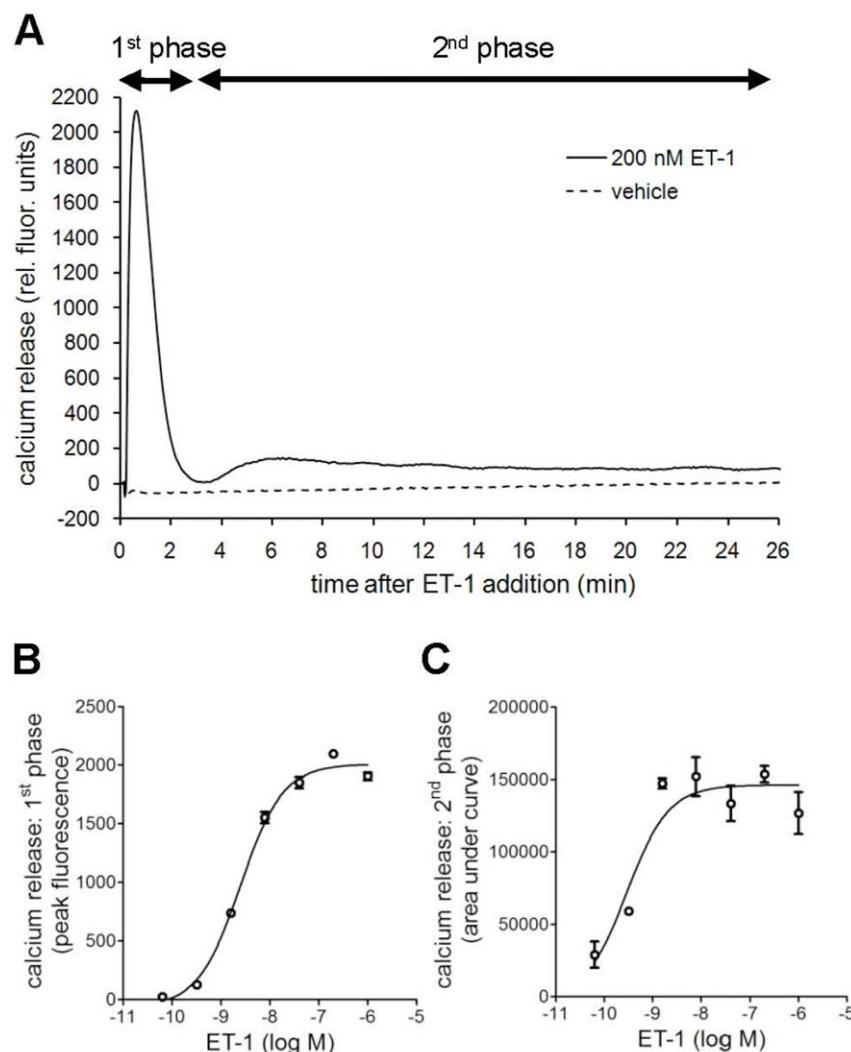
Figure 6. Characterization of the biphasic intracellular calcium response to ET-1 in PASMC. Cells were stimulated with a dilution series of ET-1 and the biphasic calcium response was recorded for 25 minutes. Shown are the raw FLIPR fluorescence traces for 200 nM ET-1 and vehicle treatment covering the first transient response phase and the second sustained response phase (A), the concentration-response-curves of ET-1 obtained for the first phase using peak fluorescence values +/− SD of duplicates (B) and the concentration-response-curves of ET-1 obtained for the second phase using area under the curve values between 3 min and 23 min after stimulation +/− SD of duplicates (C).
doi:10.1371/journal.pone.0047662.g006
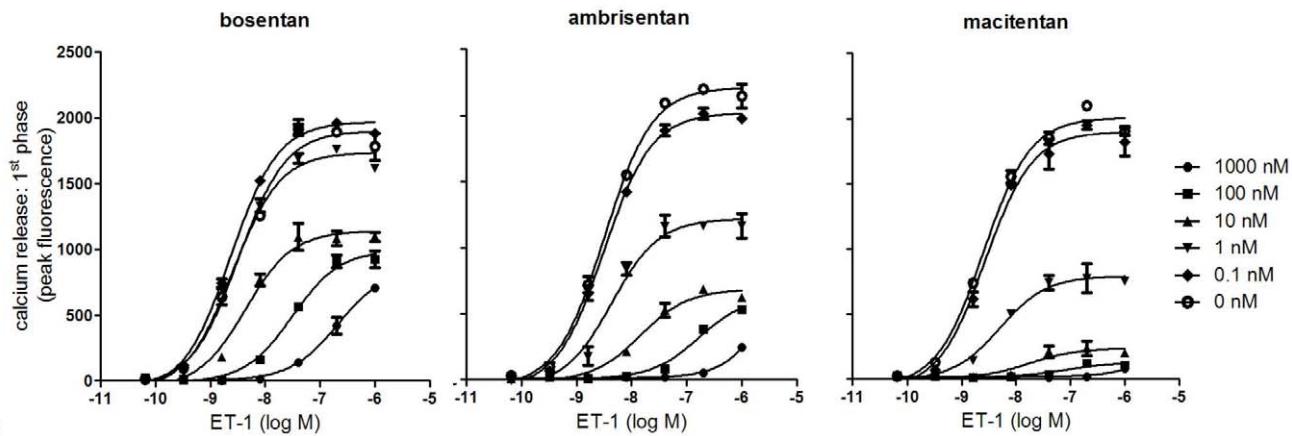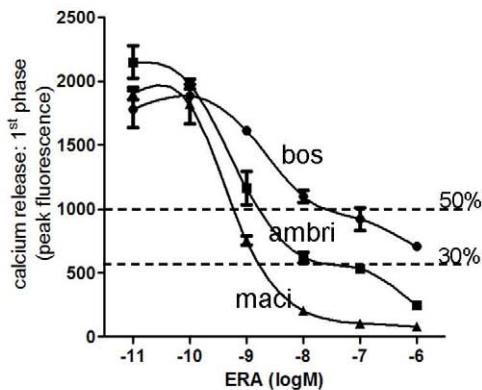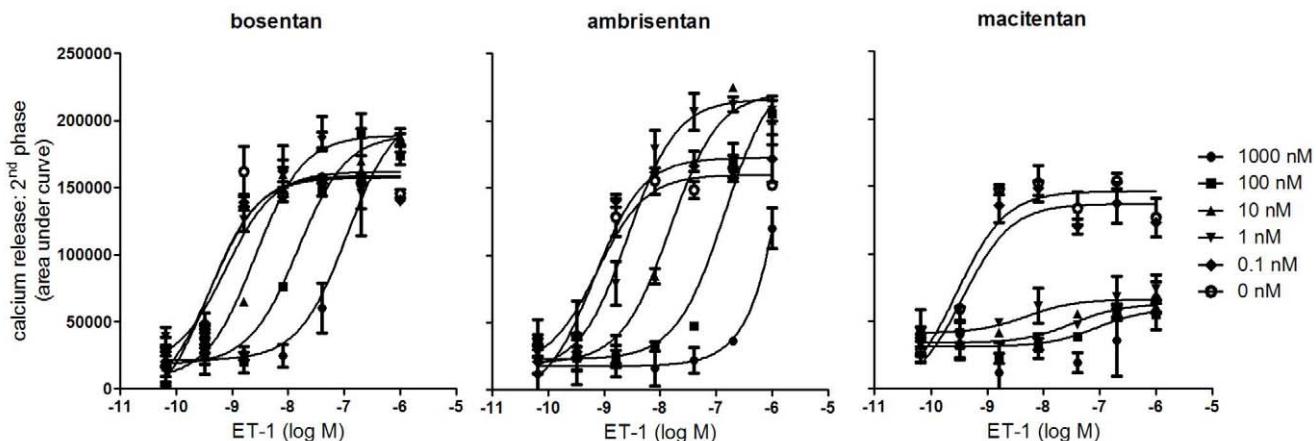
Figure 7. Effect of bosentan, ambrisentan and macitentan on both phases of the ET-1-induced calcium response. Human PASMCs were pre-incubated with dilution series of antagonists for 120 min, stimulated with a dilution series of ET-1 and the biphasic calcium response was recorded. Shown is the effect of antagonists on the ET-1 concentration-response-curves of the first response phase (A, using peak fluorescence values +/− SD of duplicates) and the second sustained response phase (C, using area under the curve values +/− SD of duplicates). Furthermore, the concentration-response-curves of the three antagonists for antagonizing peak responses induced by 1 μM ET-1 are shown +/− SD of duplicates (B) with the approximate localization of intermediate plateaus of antagonist efficacy. Shown are the results of one representative experiment out of n = 3 experiments.
doi:10.1371/journal.pone.0047662.g007

on these observations it can be estimated that within the first 30 seconds, bosentan had dissociated from ∼50% of the receptors and ambrisentan from ∼30% of receptors (assuming a 1:1 correlation between signal and receptor occupancy and lack of receptor reserve). These considerations yield a very short $ROt_{1/2}$ of <1 minute for ambrisentan and bosentan.

Fig. 7C shows the antagonistic effects of the three compounds on the second sustained phase of calcium elevation. Macitentan displayed an insurmountable mode of antagonism while the other two compounds showed surmountable antagonism. Using the Cheng-Prusoff equation, the K_b values were calculated for the first (K_{b1}, using IC_{50} values at 8 nM ET-1) and second phase (K_{b2}

using IC_{50} at 1.6 nM ET-1). Once again, macitentan (K_{b1}:0.17 nM and K_{b2} 0.093 nM) and ambrisentan (K_{b1}:0.27 nM and K_{b2}:0.14) were almost equipotent and ~10-fold more potent than bosentan (K_{b1}:2.3 nM and K_{b2}:0.79). It is interesting to note that ambrisentan and bosentan treatment did not only lack inhibitory capacity on sustained calcium release at high ET-1 concentrations, but their presence reproducibly increased the maximal efficacy of ET-1 in this readout.

Discussion

Relevance of Drug-target Binding Kinetics

The pharmacological activity of a drug depends on target affinity and on pharmacokinetic variables such as free fraction and plasma half-life and on physicochemical properties that influence the speed and degree of compound distribution into the target tissue. All of these factors are now well established and are part of any medicinal chemistry compound optimization program. However, there is increasing evidence that the kinetic behavior of the drug–target complex also influences the clinical activity of a compound [38]. Prolonged target engagement is common among effective inhibitors and in fact, of the new molecular entities approved by the FDA between 2001 and 2004, only 18% of the orthosteric inhibitors or antagonists displayed a mechanism of inhibition following purely mass action competition, whereas the majority of inhibitors (70%) were capable of sustained target blockade [39]. Thus, sustained target blockade by slow dissociation is an effective strategy to avoid or at least delay the competition between an increase in physiological ligand concentration and the drug at the target binding site. In case of strongly fluctuating ligand concentrations at the target, which can be caused by local pulsatile secretion combined with rapid degradation, sustained target blockade can lead to enhanced maximal efficacy of an inhibitor.

Many autocrine and paracrine GPCR ligands display high temporarily restricted local concentrations, and sustained receptor blockade/insurmountable antagonism seems ideally suited to enhance maximal antagonistic efficacy in such systems. Well known examples of GPCR antagonists dealing with such fluctuating para/autocrine ligands are histamine H1 antagonists (e.g. desloratidine, $ROt_{1/2}$~6 h, [40]) for the blockade of allergic responses induced by mast-cell degranulation and P_2Y_{12} antagonists (e.g. clopidogrel, irreversible binding, [41]) for the blockade of platelet aggregation induced by platelet-derived ADP. Another class of well-studied GPCR antagonists targeting an at least partially autocrine/paracrine system are the angiotensin II receptor blockers (ARBs) for the treatment of hypertension and heart disease. The slow-offset ARBs candesartan and olmesartan show increased maximal efficacy compared to the fast-offset antagonist losartan, which has a 15–25-fold shorter $ROt_{1/2}$ [37,42]. It is thus not surprising that kinetic investigations are becoming a widespread practice in modern drug discovery and may either use biochemical assays to characterize compound-target complexes or – to increase functional relevance – employ functional assays [43].

In the present study, using second messenger assays in human primary PASMC, we characterized the inhibitory potency, kinetics and mode of antagonism of macitentan, which recently concluded testing in a Phase III, long-term, event-driven, morbidity/mortality clinical trial in patients suffering from PAH. PASMC are known target cells for successful PAH therapies and endothelin-mediated effects on PASMCs were shown to contribute to PAH pathology. Two ERAs, ambrisentan and bosentan, are currently approved PAH therapies and therefore the molecular

receptor inhibition properties of macitentan were compared with those of ambrisentan and bosentan.

The ET-1-induced calcium signaling in human primary PASMC was largely ET_A driven, which was shown by using endothelin receptor subtype specific reference antagonists. The observed functional contribution of the ET_A receptor subtype in comparison to the ET_B receptor subtype was in agreement with our quantitative assessments of subtype specific mRNA expression and in agreement with the previously published reports on ET_A/ET_B expression ratios in human PASMCs [28]. In this disease-relevant primary cell system macitentan, but not ambrisentan and bosentan displayed slow receptor dissociation causing insurmountable antagonism in ET-1-induced IP_1 accumulation and ET-1-induced sustained elevation of intracellular calcium levels when ET-1 stimulation times were limited. Allowing for full equilibration of agonist and antagonist (90 min co-incubation) revealed the competitive nature of the antagonism exerted by macitentan. Our findings using second messenger assays in human primary PASMC confirm the competitive antagonism of macitentan previously shown in rat aortic ring contraction assays [30]. Since the development of vessel contraction by exogenously added ET-1 is a slow process (>100 minutes to reach EC_{50}, data not shown), contraction assays with exogenously added ET-1 do not capture the insurmountability of macitentan which occurs with short ET-1 stimulation times only.

Macitentan and ambrisentan had the same antagonistic potency in steady state assays, but showed different kinetic properties. The likely reason for this difference is different ET_A binding modes of the molecules which are a function of their molecular structure. The structure of macitentan has nothing in common with the one of ambrisentan and differs substantially from the one of bosentan, and therefore different binding modes can be expected. The ET_A receptor has been suggested to have a bitopic ET-1 binding site for accommodation of the N-terminal ET-1 address-domain and the C-terminal receptor activation domain [44]. It has furthermore been suggested that low molecular weight ERAs might display allosteric antagonism or orthosteric antagonism. The data we obtained on macitentan, ambrisentan and bosentan are highly compatible with a direct competition of these ERAs with the binding of ET-1 to either of the two parts of the bitopic binding site. Due to the kinetic and structural differences we assume that the macitentan binding site is at least partially different from the bosentan and ambrisentan binding site and that this difference in binding contributes to the slow receptor dissociation of macitentan leading to insurmountable antagonism under hemi-equilibrium conditions. A combination of molecular modeling, site directed mutagenesis, NMR and X-ray studies would be required to prove this hypothesis.

Direct Pathological Relevance in PAH of Sustained Elevation of Intracellular Calcium Levels in PASMC

This study differentiates macitentan and its mode of endothelin receptor antagonism from other ERAs using therapeutic target cells and measuring ET-1-induced second messenger levels, including the disease-relevant sustained elevation of cytosolic calcium concentrations. This sustained calcium elevation has been directly linked to sustained vessel contraction and pathological PASMC proliferation [29,36]. In PASMC, the sustained increase in cytosolic calcium is mediated via a variety of plasma membrane channels including voltage-dependent channels, store-operated channels and transient receptor potential cation channels (TRPC). Interestingly, in proliferating PASMC or PASMC from idiopathic PAH patients higher intracellular calcium levels have been observed than in growth-arrested PASMCs or PASMCs from

healthy subjects [45,46,47]. Specifically, TRPC channels have been shown to be upregulated in PAH-derived PASMC. Sustained calcium elevation is intimately linked to cellular proliferation by activation of mitogen activated protein kinases and inducing the pro-proliferative transcription factors c-jun and c-fos. Calcium also directly promotes cell cycle progression through formation of nuclear calcium-calmodulin complexes [48,49]. Therefore, highly effective blockade of ET-1-induced sustained calcium release by a slowly dissociating ERA is expected to be beneficial in inhibiting pathological proliferation of PASMC.

Advantages of a Slowly Dissociating Antagonist in the Blockade of the Paracrine/autocrine ET System

ET-1 is a paracrine/autocrine agonist released by endothelial cells, fibroblasts and smooth muscle cells in response to local stimuli such as hypoxia, growth factors or flow- and shear-stress and endothelial injury [20,21,22,23,24,25]. Importantly, besides its constitutive secretion, ET-1 can also be released from specialized storage vesicles, so called Weibel-Palade bodies, which concentrate and store ET-1 beneath the plasma membrane of endothelial cells [17,18]. Constitutive and stimulated ET-1 secretory mechanisms are complemented by highly effective local ET-1 degrading enzymes as evidenced by very short half lives of free ET-1 in tissue extracts [50,51,52,53]. The spatial and temporal pattern of ET-1 release and degradation in diseased tissue and the resulting local ET-1 concentration-time profiles encountered by PASMC, cardiomyocytes, cardiac and lung fibroblasts are still unknown. However, under the assumption of fluctuating, i.e. not equilibrated local ET-1 concentrations in vivo, a slowly dissociating antagonist such as macitentan is expected to display a more complete block of ET-1 binding to its receptors than ambrisentan and bosentan. Furthermore, it is likely that the ET-1 that is prevented from binding to the blocked ET receptors is rapidly degraded and not available for renewed binding attempts.

Conclusions

Macitentan is differentiated from the two currently approved ERAs through its slower receptor dissociation kinetics and insurmountable antagonism in non-equilibrium assays. Under conditions of local ET-1 fluctuations *in vivo*, macitentan should block ET-1-induced signaling more effectively than other ERAs. These qualities may contribute to a unique effectiveness of macitentan in diseases characterized by increased autocrine and paracrine ET-1 signaling such as PAH.

Materials and Methods

Cell Culture

Chinese hamster ovary (CHO) cells recombinantly expressing ET_A or ET_B receptors were cultivated in growth medium [Ham F-12 with L-glutamine containing 1000 µg/mL G418, 100 U/mL penicillin, 100 µg/mL streptomycin, and 10% heat-inactivated fetal calf serum (FCS)]. PASMC were purchased from TCS Cellworks (ZHC-3116) and cultivated in growth medium (Lonza Clonetics SmBM (CC-3181)) with SmGM-2 SingleQuots supplements and 5% FCS (CC-4149)). PASMC of passage 3 to 5 were used for all experiments.

ERAs

Macitentan, bosentan, ambrisentan, and tezosentan were synthesized by Actelion Pharmaceuticals Ltd., sitaxentan was purchased from Convertex (Germany) and zibotentan from Acesys Pharmatech (USA). BQ-123 and BQ-788 were or purchased from Sigma.

Intracellular Calcium Release Measurements Using Recombinant CHO-ET_A and CHO-ET_B Cells

CHO-ET_A or CHO-ET_B cells were seeded in growth medium at 20,000 cells/well into 384-well black clear-bottom sterile plates (Greiner) and incubated overnight at 37°C in 5% CO_2. Then, the growth medium was exchanged by 50 µL/well of dye buffer [HBSS, 0.1% bovine serum albumin (BSA), 20 mM HEPES, 0.375 g/L $NaHCO_3$, 5 mM probenecid (Sigma), 1% FCS and 3 µM fluo-4 AM]. Cells were incubated for 1 h at 37°C in 5% CO_2 followed by equilibration at room temperature for at least 30 min. Then, within the Fluorescent Imaging Plate Reader (FLIPR Tetra, Molecular Devices), plates were subjected to protocols consisting of two additions of 10 µL each for the determination of the inhibitory potency (IC_{50} and K_b) of the endothelin receptor antagonists. Calcium traces were recorded and then processed as described below. For the determination of antagonistic potency of endothelin receptor antagonists (K_b) cells were supplemented with 10 µL of 6× concentrated antagonist dilution series prepared in assay buffer covering the final concentration range from 0 nM to 10 µM (0.5% DMSO final assay concentration). After a 120-min incubation at room temperature, cells were stimulated by the addition of 10 µL of 7× concentrated ET-1 to obtain an assay concentration of EC_{50}–EC_{70}. Calcium release was monitored for 3 min. For the K_b calculations, FLIPR traces were subjected to spatial uniformity correction and normalized by trace alignment at the last time point before agonist addition (ScreenWorks software, Molecular Devices). Then, relative fluorescence units (RFU) of the maximum signal per well were exported and used by the proprietary IC_{50} Witch software to calculate IC_{50} values (settings for IC_{50} values = use of fixed minimum (10 µM macitentan) and curve-intrinsic maximum). K_b values were calculated via the Cheng-Prusoff equation $[K_b = IC_{50}/(1+ [ET-1_{stim}]/EC_{50\_ET-1})]$ using the determined IC_{50} values, the EC_{50} of ET-1 (determined daily), and the ET-1 stimulating concentration used [31].

Intracellular Calcium Release Measurements Using Human PASMC

PASMC were seeded in growth medium at 8,000 cells/well (exception sustained calcium release, see below) into 384-well black clear-bottom sterile plates (Greiner) and incubated overnight at 37°C in 5% CO_2. Then, cell culture medium was exchanged by 50 µL/well of dye buffer [HBSS, 0.1% BSA, 20 mM HEPES, 0.375 g/L $NaHCO_3$, 5 mM probenecid (Sigma) and 3 µM of fluo-4 AM]. The cell plates were incubated for 1 h at 37°C in 5% CO_2 followed by equilibration at room temperature for at least 30 min. Within the FLIPR, plates were subjected to protocols consisting of two additions of 10 µL each, either for the determination of the inhibitory potency (IC_{50} and K_b) of the endothelin receptor antagonists, for the analysis of antagonist $ROt_{1/2}$, or for the analysis of sustained calcium fluxes. Calcium traces were recorded and processed as described below. For the K_b determinations, cells were supplemented with 10 µL of 6× concentrated antagonist dilution series prepared in assay buffer covering the final concentration range from 0 nM to 1 µM. The final assay concentration of DMSO was 0.1%. After 10 min or 120 min at room temperature, cells were stimulated with ET-1 by the addition of 10 µL of 7× concentrated ET-1 to obtain a final concentration of EC_{50}–EC_{70}. Calcium release was monitored for 3 min. For the K_b calculations, FLIPR traces were subjected to spatial uniformity correction and normalized by trace alignment at the last time point before agonist addition (ScreenWorks software, Molecular Devices). Then, RFU of the maximum signal per well

were exported and used by the proprietary IC_{50} Witch software to calculate IC_{50} values [settings for IC_{50} values = use of fixed minimum (1 µM macitentan, always causing full signal blockade) and curve-intrinsic maximum]. K_b values were calculated via the Cheng-Prusoff equation using the determined IC_{50} values, the acutely determined EC_{50} of ET-1, and the ET-1 stimulating concentration used. For the determination of $ROt_{1/2}$ values of the different ERA, cells were supplemented with 10 µL of antagonist dilution series and incubated at room temperature for 120 min. Then, cells were either stimulated in the FLIPR by the addition of 10 µL of 7× concentrated ET-1 (final assay concentration EC_{50}–EC_{70}), or cells were washed twice with 50 µL/well assay buffer (HBSS containing 0.1% BSA, 20 mM HEPES, 0.375 g/L $NaHCO_3$, 2.5 mM probenecid, pH 7.4). After 5, 10, 20, 30 and 60 min of incubation at room temperature, cells were stimulated with an EC_{50}–EC_{70} of ET-1 by the addition of 10 µL of a 7× concentrated ET-1 stock in assay buffer. Calcium release was monitored for 3 min. For the estimation of receptor $ROt_{1/2}$, the K_b values were calculated via the Cheng-Prusoff equation using on-plate generated EC_{50} values of ET-1, and the earliest time point with a K_b value significantly shifted versus the non-washed control K_b value ($K_{b0\ min}$) was used. Significant change from $K_{b0\ min}$ ($p<0.05$) was determined using the one-way ANOVA test including Dunnett's post test using GraphPadPrism software and is indicated with an asterisk in Fig. 3. An approximate $ROt_{1/2}$ was then calculated assuming first order dissociation kinetics: $t_{1/2} = t_x/[\log_2 (K_{bxmin}/K_{b0\ min})]$ with x = time point of first significant change in K_b after wash-out.

For the determination of antagonistic effects on ET-1-induced sustained intracellular calcium release, PASMC were seeded in growth medium at 20,000 cells/well into FLIPR plates. After 1.5 h of attachment at 37°C/5% CO_2, medium was exchanged with 50 µL/well of starvation medium (SmBM containing 1/10 of usual supplement concentrations). The next day, cells were dyed as described above and then supplemented with 10 µL of 6× concentrated dilution series of ERAs in assay buffer covering assay concentrations between 0 nM and 1 µM. The final DMSO concentration in the assay was 0.1%. After 120 min of incubation at room temperature, cells were stimulated by the addition of 10 µL of a 7× concentrated dilution series of ET-1 in assay buffer covering assay concentrations between 0 nM and 1 µM. Assay buffer in this assay type contained 2.5 mM probenecid. Intracellular calcium elevation was monitored for 25 min. The ERA effects on the first response phase were analyzed by calculating the K_b value from the IC_{50} generated at 8 nM ET-1 concentation. For the analysis of sustained calcium-response, FLIPR traces were subjected to spatial uniformity correction and normalized by trace alignment at the last time point before agonist addition (Screen-Works software, Molecular Devices). Sustained calcium release was quantified by calculating the area under the FLIPR trace (area under the curve = AUC) between 3 min and 23 min after ET-1 addition. In addition, the IC_{50} value at 1.6 nM ET-1 stimulating concentration was determined using the proprietary IC_{50} Witch software (settings for IC_{50} values = use of fixed minimum (non-stimulated control) and curve-intrinsic maximum). K_b values were calculated via the Cheng-Prusoff equation using the determined IC_{50} values, the acutely determined EC_{50} of ET-1, and the ET-1 stimulating concentration used (1.6 nM).

References

1. Galiè N, Hoeper MM, Humbert M, Torbicki A, Vachiery JL, et al. (2009) Guidelines for the diagnosis and treatment of pulmonary hypertension: the Task Force for the Diagnosis and Treatment of Pulmonary Hypertension of the European Society of Cardiology (ESC) and the European Respiratory Society (ERS), endorsed by the International Society of Heart and Lung Transplantation (ISHLT). Eur Heart J 30: 2493–2537.

IP_1 Measurements

All measurements were performed using the IP-One HTRF kit (Cisbio, #62IPAPEC) following the manufacturers protocol. PASMC were seeded at 10,000 cells/20 µL/well into 384-well, white, small-volume, tissue culture sterile plates (Greiner #784080) and incubated overnight at 37°C in 5% CO_2. Then, medium was removed and 5 µL/well of assay buffer (HBSS containing 0.1% BSA, 20 mM HEPES, 0.375 g/L $NaHCO_3$, 50 mM LiCl, pH 7.4) were added. Then, cells were supplemented with 5 µL/well of a 2× concentrated dilution series of antagonists in assay buffer covering a fincal concentration range of 0–10 µM and incubated for 120 min at 37°C in 5% CO_2. Then, 2.5 µL/well of 5× concentrated solutions of ET-1 in assay buffer covering a final concentration range of 0–5 µM were added followed by an incubation at 37°C/5% CO_2 for either 20 min or 90 min. Cells were lysed by the addition of 2.5 µL/well of conjugate-lysis buffer. Then, 2 µL/well of IP_1-d2 conjugate and 3 µL/well of anti-IP_1-cryptate terbium were added, and after 60 min incubation at room temperature, the assay plates were excited at 337 nm and the ratio of emitted light at 665 nm and 620 nm was recorded using the PHERAstar (BMG labtech). 665 nm/620 nm emission ratios were translated into IP_1 concentrations via an on-plate calibration curve generated with known concentrations of IP_1. IP_1 concentration values were exported into GraphPadPrism software and the ET-1 concentration-response curves (CRC) in the presence of different antagonist concentrations were fitted by non-linear regression using the Gaddum/Schild analysis function for surmountable antagonism. The ET-1 CRC after 20-min stimulation in the presence of macitentan showed insurmountable antagonism and were fitted by the 3-parameter non-linear regression function of GraphPadPrism. To average the independent experiments, IP_1 concentrations were normalized per experiment using the maximal response to ET-1 in the absence of antagonist as reference point. K_b values for the 20-min stimulation with ET-1 were obtained via the Cheng-Prusoff equation from the calculated IC_{50} value at 1.6 nM ET-1 [settings for IC_{50} calculation: curve intrinsic minimum (non-stimulated control) and curve-intrinsic maximum], the EC_{50} of ET-1 and the stimulating ET-1 concentration (1.6 nM). Schild K_b values for the 90-min stimulation with ET-1 (all ERAs were surmountable) were generated by the GraphPadPrism software after applying the Gaddum/Schild non-linear regression function. K_b values are expressed as geometric means of 3–4 independent measurements including the geometric standard deviation σ_g which is calculated from the standard deviation SD of the pK_b values as follows $\sigma_g = 10\exp(SD_{pKb})$.

Acknowledgments

Author Contributions

Conceived and designed the experiments: JG. Performed the experiments: CMG TS. Analyzed the data: CMG TS JG. Wrote the paper: JG ON MC.

2. Tuder RM, Cool CD, Yeager M, Taraseviciene-Stewart L, Bull TM, et al. (2001) The pathobiology of pulmonary hypertension. Endothelium. Clin Chest Med 22: 405–418.

3. Morrell NW, Adnot S, Archer SL, Dupuis J, Jones PL, et al. (2009) Cellular and molecular basis of pulmonary arterial hypertension. J Am Coll Cardiol 54: S20–31.

4. Archer SL, Weir EK, Wilkins MR (2010) Basic science of pulmonary arterial hypertension for clinicians: new concepts and experimental therapies. Circulation 121: 2045–66.

5. Humbert M, Sitbon O, Chaouat A, Bertocchi M, Habib G, et al. (2010) Survival in patients with idiopathic, familial, and anorexigen-associated pulmonary arterial hypertension in the modern management era. Circulation 122: 156–163.

6. Giaid A, Yanagisawa M, Langleben D, Michel RP, Levy R, et al. (1993) Expression of endothelin-1 in the lungs of patients with pulmonary hypertension. N Engl J Med 328: 1732–1739.

7. Shao D, Park JE, Wort SJ (2011) The role of endothelin-1 in the pathogenesis of pulmonary arterial hypertension. Pharmacol Res 63: 504–511.

8. Schiffrin EL, Touyz RM (1998) Vascular biology of endothelin. J Cardiovasc Pharmacol 32: S2–13.

9. Iglarz M, Clozel M (2007) Mechanisms of ET-1-induced endothelial dysfunction. J Cardiovasc Pharmacol 50: 621–628.

10. Price LC, Howard LS (2008) Endothelin receptor antagonists for pulmonary arterial hypertension: rationale and place in therapy. Am J Cardiovasc Drugs 8: 171–185.

11. Komuro I, Kurihara H, Sugiyama T, Yoshizumi M, Takaku F, et al. (1988) Endothelin stimulates c-fos and c-myc expression and proliferation of vascular smooth muscle cells. FEBS Lett 238: 249–252.

12. Salani D, Taraboletti G, Rosanò L, Di Castro V, Borsotti P, et al. (2000) Endothelin-1 induces an angiogenic phenotype in cultured endothelial cells and stimulates neovascularization in vivo. Am J Pathol 157: 1703–1711.

13. Leask A (2011) The role of endothelin-1 signaling in the fibrosis observed in systemic sclerosis. Pharmacol Res 63: 502–503.

14. Hosoda K, Nakao K, Arai H, Suga S, Ogawa Y, et al. (1991) Cloning and expression of human endothelin-1 receptor cDNA. FEBS Lett 287: 23–26.

15. Ogawa Y, Nakao K, Arai H, Nakagawa O, Hosoda K, et al. (1991) Molecular cloning of a non-isopeptide-selective human endothelin receptor. Biochem Biophys Res Commun 178: 248–255.

16. Bouallegue A, Daou GB, Srivastava AK (2007) Endothelin-1-induced signaling pathways in vascular smooth muscle cells. Curr Vasc Pharmacol 5: 45–52.

17. Russell FD, Skepper JN, Davenport AP (1998) Evidence using immunoelectron microscopy for regulated and constitutive pathways in the transport and release of endothelin. J Cardiovasc Pharmacol 31: 424–430.

18. Russell FD, Davenport AP (1999) Secretory pathways in endothelin synthesis. Br J Pharmacol 126: 391–398.

19. Wagner OF, Christ G, Wojta J, Vierhapper H, Parzer S, et al. (1992) Polar secretion of endothelin-1 by cultured endothelial cells. J Biol Chem 267: 16066–16068.

20. Yamashita K, Discher DJ, Hu J, Bishopric NH, Webster KA (2001) Molecular regulation of the endothelin-1 gene by hypoxia. Contributions of hypoxia-inducible factor-1, activator protein-1, GATA-2, AND p300/CBP. J Biol Chem 276: 12645–12653.

21. Kanse SM, Takahashi K, Warren JB, Ghatei M, Bloom SR (1991) Glucocorticoids induce endothelin release from vascular smooth muscle cells but not endothelial cells. Eur J Pharmacol 199: 99–101.

22. Rodríguez-Pascual F, Reimunde FM, Redondo-Horcajo M, Lamas S (2004) Transforming growth factor-beta induces endothelin-1 expression through activation of the Smad signaling pathway. J Cardiovasc Pharmacol 44: S39–42.

23. Malek AM, Greene AL, Izumo S (1993) Regulation of endothelin 1 gene by fluid shear stress is transcriptionally mediated and independent of protein kinase C and cAMP. Proc Natl Acad Sci U S A 90: 5999–6003.

24. Malek AM, Zhang J, Jiang J, Alper SL, Izumo S (1999) Endothelin-1 gene suppression by shear stress: pharmacological evaluation of the role of tyrosine kinase, intracellular calcium, cytoskeleton, and mechanosensitive channels. J Mol Cell Cardiol 31: 387–399.

25. Woods M, Mitchell JA, Wood EG, Barker S, Walcot NR, et al. (1999) Endothelin-1 is induced by cytokines in human vascular smooth muscle cells: evidence for intracellular endothelin-converting enzyme. Mol Pharmacol 55: 902–909.

26. Haynes WG, Webb DJ (1998) Endothelin as a regulator of cardiovascular function in health and disease. J Hypertens 16: 1081–1098.

27. Janakidevi K, Fisher MA, Del Vecchio PJ, Tiruppathi C, Figge J, et al. (1992) Endothelin-1 stimulates DNA synthesis and proliferation of pulmonary artery smooth muscle cells. Am J Physiol 263: C1295–1301.

28. Davie N, Haleen SJ, Upton PD, Polak JM, Yacoub MH, et al. (2002) ET(A) and ET(B) receptors modulate the proliferation of human pulmonary artery smooth muscle cells. Am J Respir Crit Care Med 165: 398–405.

29. Tajsic T, Morrell NW (2010) Smooth Muscle Cell Hypertrophy, Proliferation, Migration and Apoptosis in Pulmonary Hypertension. Compr Physiol: 295–317.

30. Iglarz M, Binkert C, Morrison K, Fischli W, Gatfield J, et al. (2008) Pharmacology of macitentan, an orally active tissue-targeting dual endothelin receptor antagonist. J Pharmacol Exp Ther 327: 736–745.

31. Cheng Y, Prusoff WH (1973) Relationship between the inhibition constant (K_I) and the concentration of inhibitor which causes 50 per cent inhibition (I_{50}) of an enzymatic reaction. Biochem Pharmacol 22: 3099–3108.

32. Kenakin T, Jenkinson S, Watson C (2006) Determining the potency and molecular mechanism of action of insurmountable antagonists. J Pharmacol Exp Ther 319: 710–723.

33. Pollock DM, Keith TL, Highsmith RF (1995) Endothelin receptors and calcium signaling. FASEB J 9: 1196–1204.

34. Shimoda LA, Sylvester JT, Sham JS (2000) Mobilization of intracellular Ca(2+) by endothelin-1 in rat intrapulmonary arterial smooth muscle cells. Am J Physiol Lung Cell Mol Physiol 278: L157–164.

35. Schroeder AC, Imig JD, LeBlanc EA, Pham BT, Pollock DM, et al. (2000) Endothelin-mediated calcium signaling in preglomerular smooth muscle cells. Hypertension 35: 280–286.

36. Kuhr FK, Smith KA, Song MY, Levitan I, Yuan JX (2012) New mechanisms of pulmonary arterial hypertension: role of Ca^{2+} signaling. Am J Physiol Heart Circ Physiol 302: H1546–1562.

37. Le MT, Pugsley MK, Vauquelin G, Van Liefde I (2007) Molecular characterisation of the interactions between olmesartan and telmisartan and the human angiotensin II AT1 receptor. Br J Pharmacol 151: 952–962.

38. Vauquelin G, Charlton SJ (2010) Long-lasting target binding and rebinding as mechanisms to prolong in vivo drug action. Br J Pharmacol 161: 488–508.

39. Swinney DC (2006) Biochemical mechanisms of New Molecular Entities (NMEs) approved by United States FDA during 2001–2004: mechanisms leading to optimal efficacy and safety. Curr Top Med Chem 6: 461–478.

40. Anthes JC, Gilchrest H, Richard C, Eckel S, Hesk D, et al. (2002) Biochemical characterization of desloratadine, a potent antagonist of the human histamine H(1) receptor. Eur J Pharmacol 449: 229–37.

41. Herbert JM, Savi P (2003) P2Y12, a new platelet ADP receptor, target of clopidogrel. Semin Vasc Med 3: 113–122.

42. Gradman AH (2002) AT(1)-receptor blockers: differences that matter. J Hum Hypertens 16: S9–S16.

43. Casarosa P, Kollak I, Kiechle T, Ostermann A, Schnapp A, et al. (2011) Functional and biochemical rationales for the 24-hour-long duration of action of olodaterol. J Pharmacol Exp Ther 337: 600–609.

44. De Mey JG, Compeer MG, Lemkens P, Meens MJ (2011) ETA-receptor antagonists or allosteric modulators? Trends Pharmacol Sci 32: 345–351.

45. Yuan JX, Aldinger AM, Juhaszova M, Wang J, Conte JV Jr, et al. (1998) Dysfunctional voltage-gated K+ channels in pulmonary artery smooth muscle cells of patients with primary pulmonary hypertension. Circulation 98: 1400–1406.

46. Golovina VA, Platoshyn O, Bailey CL, Wang J, Limsuwan A, et al. (2001) Upregulated TRP and enhanced capacitative Ca(2+) entry in human pulmonary artery myocytes during proliferation. Am J Physiol Heart Circ Physiol 280: H746–755.

47. Platoshyn O, Golovina VA, Bailey CL, Limsuwan A, Krick S, et al. (2000) Sustained membrane depolarization and pulmonary artery smooth muscle cell proliferation. Am J Physiol Cell Physiol 279: C1540–1549.

48. Berridge MJ (1993) Inositol trisphosphate and calcium signalling. Nature 361: 315–25.

49. Hardingham GE, Chawla S, Johnson CM, Bading H (1997) Distinct functions of nuclear and cytoplasmic calcium in the control of gene expression. Nature 385: 260–265.

50. Dickinson KE, Tymiak AA, Cohen RB, Liu EC, Webb ML, et al. (1991) Vascular A10 cell membranes contain an endothelin metabolizing neutral endopeptidase. Biochem Biophys Res Commun 176: 423–430.

51. Edano T, Arai K, Ohshima T, Koshi T, Hirata M, et al. (1994) Purification and characterization of endothelin-1 degradation activity from porcine kidney. Biol Pharm Bull 17: 379–382.

52. Battistini B, Brown M, Vane JR (1995) Selective proteolitic activation and degradation of ETs and big ETs in parenchymal strips of the guinea-pig lung. Biochem Biophys Res Commun 207: 675–81.

53. Pérez-Vizcaíno F, Cooper AC, Corder R, Fournier A, Warner TD (1995) Rapid degradation of endothelin-1 by an enzyme released by the rat isolated perfused mesentery. Br J Pharmacol 114: 867–871.